Volume 19 | Number 10 | 14 March 2017 | Pages 6891–7432

PCCP

Physical Chemistry Chemical Physics

rsc.li/pccp

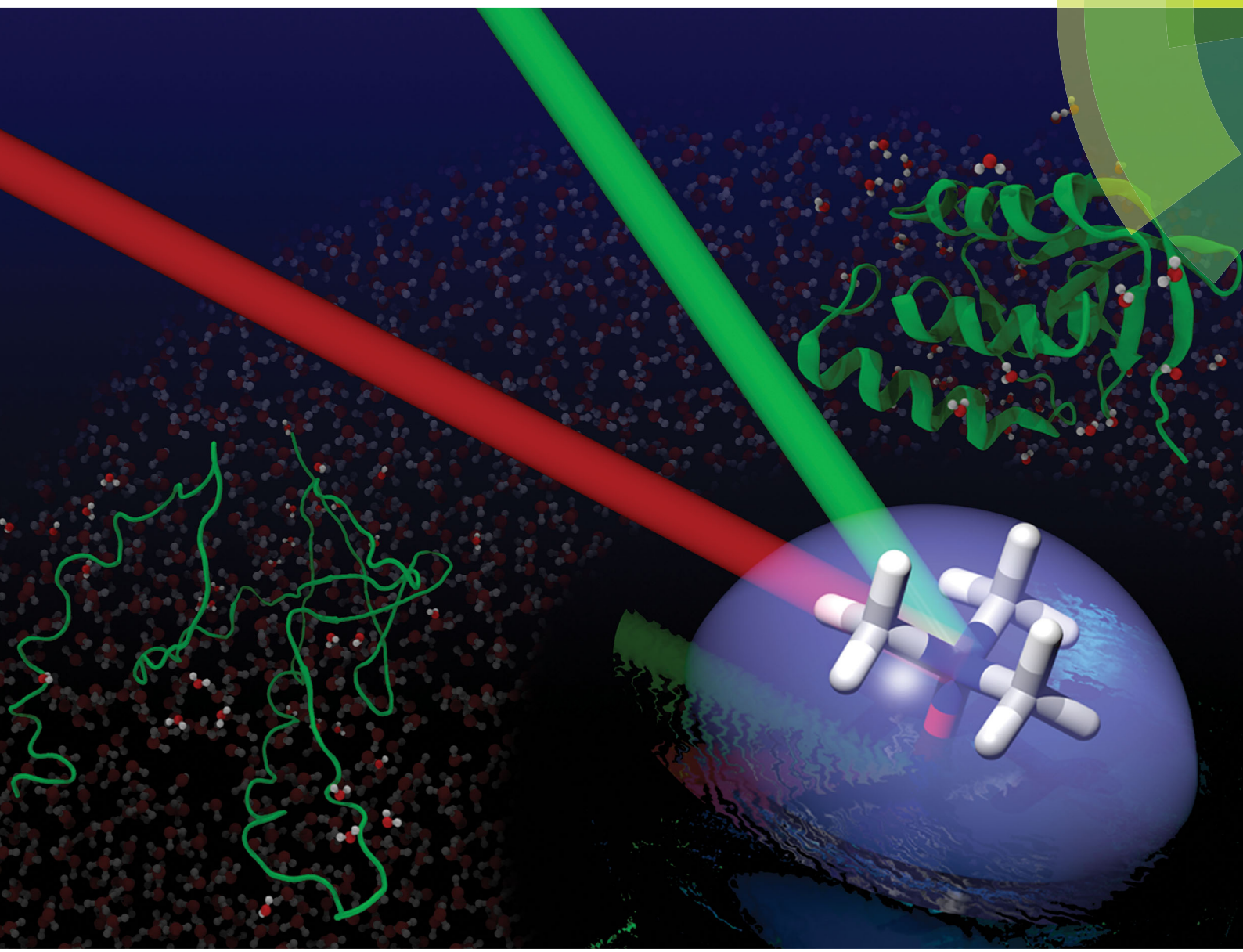

ISSN 1463-9076

ROYAL SOCIETY OF CHEMISTRY

PERSPECTIVE

Yuki Nagata *et al.*

Trimethylamine-*N*-oxide: its hydration structure, surface activity, and biological function, viewed by vibrational spectroscopy and molecular dynamics simulations

PCCP

PERSPECTIVE

View Article Online
View Journal | View Issue

Cite this: *Phys. Chem. Chem. Phys.*, 2017, **19**, 6909

Trimethylamine-*N*-oxide: its hydration structure, surface activity, and biological function, viewed by vibrational spectroscopy and molecular dynamics simulations

Tatsuhiko Ohto,[a] Johannes Hunger,[b] Ellen H. G. Backus,[b] Wataru Mizukami,[c] Mischa Bonn[b] and Yuki Nagata*[bd]

Received 24th October 2016,
Accepted 11th January 2017

DOI: 10.1039/c6cp07284d

rsc.li/pccp

The osmolyte molecule trimethylamine-*N*-oxide (TMAO) stabilizes the structure of proteins. As functional proteins are generally found in aqueous solutions, an important aspect of this stabilization is the interaction of TMAO with water. Here, we review, using vibrational spectroscopy and molecular dynamics simulations, recent studies on the structure and dynamics of TMAO with its surrounding water molecules. This article ends with an outlook on the open questions on TMAO–protein and TMAO–urea interactions in aqueous environments.

I. Introduction

Trimethylamine-*N*-oxide (TMAO) is a small zwitterionic molecule in which the oxygen (O_{TMAO}) and nitrogen (N_{TMAO}) atoms are negatively and positively charged, respectively. This O–N group can be considered as the hydrophilic part of the molecule. The rest of the TMAO molecule is composed of three methyl groups and can thus be considered as the hydrophobic part. This is the reason for TMAO being called an amphiphilic molecule.

[a] *Graduate School of Engineering Science, Osaka University, 1-3 Machikaneyama, Toyonaka, Osaka 560-8531, Japan*
[b] *Max Planck Institute for Polymer Research, Ackermannweg 10, 55128 Mainz, Germany. E-mail: nagata@mpip-mainz.mpg.de*
[c] *Department of Energy and Material Sciences, Faculty of Engineering Sciences, Kyushu University, 6-1 Kasuga-Park, Fukuoka, 816-8580, Japan*
[d] *Department of Theoretical and Computational Molecular Science, Institute for Molecular Science, Myodaiji, Okazaki, Aichi, 444-8585, Japan*

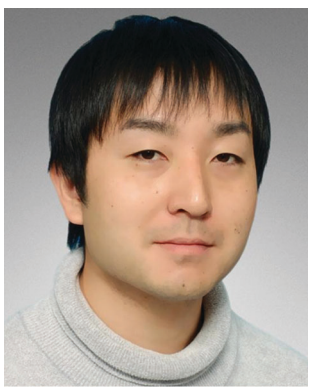

Tatsuhiko Ohto

Tatsuhiko Ohto is an assistant professor at Osaka University, Osaka, Japan. He received his PhD degree from The University of Tokyo in 2013. During his PhD course, he spent 5 months as a visiting student at the Max Planck Institute for Polymer Research, Mainz, Germany. After postdoctoral research at the Advanced Institute of Science and Technology, Tsukuba, Japan, he joined Osaka University. His research interest is theoretical modeling, primarily based on first-principles calculations, of the structure and dynamics of molecules at interfaces and the electron transport of metal–molecule–metal systems.

Johannes Hunger

Johannes Hunger studied chemistry at the University of Regensburg, Germany, from where he obtained his degree in 2006. Then he joined Prof Buchner's group at the University of Regensburg for his PhD project on the effect of polar compounds on the dynamics of ionic liquids. In 2010 he moved to the FOM Institute AMOLF (Amsterdam, Netherlands) for his postdoctoral studies on the dynamics in aqueous solutions using ultrafast laser spectroscopy. Since February 2012 he has led the liquid dynamics group at the Max Planck Institute for Polymer Research. His current research focuses on ionic and hydrogen-bonding interactions in solutions with relevance to catalysis, cellulose processing, waste treatment, and solar energy harvesting.

TMAO also serves as an osmolyte, enabling, for instance, marine organisms to adjust their osmotic pressure. In fact, sharks contain both urea and TMAO.[1,2] Although both urea and TMAO function as osmolytes, the effects of these molecules on protein stability are opposite. TMAO stabilizes the structure of proteins, while urea destabilizes them. It has been believed that by balancing the destabilization effects of urea with the stabilization effects of TMAO, living organisms which contain both TMAO and urea can maintain their protein structure and at the same time adjust the osmotic pressure.[1]

To understand the biological function of TMAO, one should understand the solvation structure of TMAO, the nature and strength of the interaction of TMAO with proteins, and the conformations of TMAO and urea in an aqueous environment not only under ambient conditions but also under extreme conditions such as at high pressure.[3,4] Typical questions regarding TMAO are: although TMAO is known to be an amphiphilic molecule, to what extent is the methyl group of TMAO hydrophobic? How do the surrounding water molecules interact with a TMAO molecule? How does TMAO interact with urea? How does TMAO stabilize the structure of a protein? Infrared (IR) spectroscopy,[5–8] Raman spectroscopy,[9,10] nuclear magnetic resonance spectroscopy,[11,12] X-ray spectroscopy,[13,14] dielectric relaxation spectroscopy,[5,15] and molecular dynamics (MD) simulations[16–18] have been used to address these questions.

These reports contain different views of TMAO. For example, the slowing down of the water motion near TMAO has been attributed to the hydrophobic hydration of the methyl groups of

Ellen H. G. Backus

Ellen H. G. Backus is leading the "Water at Interfaces" group in the Molecular Spectroscopy Department at the Max Planck Institute for Polymer Research (MPIP), Mainz. She obtained her PhD in 2005 from Leiden University, in the group of Mischa Bonn and Aart Kleyn. After working as a postdoctoral researcher at the University of Zurich with Peter Hamm, she moved back to the Netherlands for an independent postdoctoral researcher position in the group of Huib Bakker at AMOLF in Amsterdam. In 2012, she joined the MPIP. The research aim of the group is to understand the structure and dynamics of water at the molecular level at various interfaces.

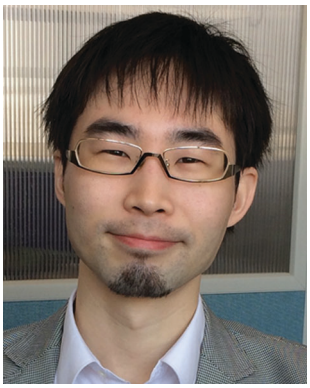

Wataru Mizukami

Wataru Mizukami obtained his Bachelor degree from Kyoto University and Masters from the University of Tokyo. He received his PhD in physics from the Graduate University for Advanced Studies in Japan under the supervision of Dr Takeshi Yanai (2011). He worked with Dr David Tew in Bristol as a Marie Curie fellow. In 2014, he worked at RIKEN, Japan as a PD, under the supervision of Dr Yuji Sugita. Since 2015, he has been working at Kyushu University as an assistant professor. His research focuses on the development and application of electronic and vibrational structure theory for molecules.

Mischa Bonn

Mischa Bonn is a director at the Max-Planck Institute for Polymer Research (MPIP), Mainz, Germany. He works on label-free (ultrafast) vibrational spectroscopy and microscopy of biomolecular systems and water in such systems. He received his PhD in 1996 from the University of Eindhoven for research performed at the FOM-Institute for Atomic and Molecular Physics AMOLF in Amsterdam. After postdoctoral research at the Fritz Haber Institute in Berlin and Columbia University in New York, he worked at Leiden University from 1999 as an assistant professor, and from 2002 as an associate professor. In 2004 he became a group leader at the AMOLF. In 2011 he joined MPIP. His research interests are the structure and dynamics of molecules at interfaces, and electron transfer across interfaces.

Yuki Nagata

Yuki Nagata is a group leader of the Max Planck Institute for Polymer Research, Mainz, Germany. He received his Bachelor and Master degrees from the University of Tokyo, and his PhD degree from Kyoto University. He worked as a research scientist at the BASF SE and a postdoctoral researcher at the group of Prof Mukamel, University of California, Irvine. In 2011, he joined the Max-Planck Institute for Polymer Research. In 2016, he was also assigned as a visiting associate professor, Institute for Molecular Science, Okazaki, Japan. His research focus is on the molecular mechanism of the aqueous interface and the theoretical design of vibrational spectroscopy.

TMAO[6] or strong hydrogen bonds between water and the hydrophilic oxygen atom.[19] In contrast to the dynamics of water near the methyl groups of TMAO, the structure of water in an aqueous TMAO solution has been found to be very similar to that of neat water.[20–24] Moreover, the nature of the TMAO methyl group – hydrophilic or hydrophobic – has been debated.[25–27] To resolve these apparent contradictions, new technologies have been used to study aqueous TMAO solutions: beyond the classical force field MD simulations, *ab initio* MD (AIMD) simulations[28] have been employed. Experimentally, beyond the linear vibrational spectroscopy, surface-specific, time-resolved, two-dimensional vibrational spectroscopy[29] has been used. More importantly, the combination of simulations and advanced spectroscopy has potential for providing a unified picture of TMAO.

In this review, we provide an overview of the recent studies on TMAO using vibrational spectroscopy and/or MD simulations. In Section II, the vibrational frequency assignment of TMAO C–H stretching modes and the frequency modulation of the water O–H stretching modes due to the presence of TMAO are discussed. In Section III, the spectroscopic investigation on the TMAO hydration structure and dynamics is introduced. Furthermore, recent efforts towards understanding these spectroscopic data based on MD simulations are also reviewed. Section IV explains the study to examine the hydrophilicity of TMAO using surface-specific sum-frequency generation (SFG) spectroscopy. We end with an outlook and challenges in understanding the complex interplay of TMAO, urea, and proteins.

II. Fundamental properties of TMAO molecules

II-A. Electronic structure of TMAO

In this section, we summarize the molecular properties of TMAO by comparing it with *tert*-butyl alcohol (TBA). Fig. 1 displays the molecular structures of TMAO and TBA. Both molecules have three methyl groups, while TMAO has a zwitterionic N^+–O^- group and TBA has a C–O–H hydroxyl group. Although the chemical compositions of TMAO and TBA are similar, the molecular properties are very different. The calculated dipole moment of TBA is 1.49 Debye at the M06/cc-pVTZ level of theory calculated using the GAMESS code,[30] while the dipole moment of TMAO is 4.55 Debye, much larger than that of TBA. Due to this large difference in the dipole moment, TBA aggregates in aqueous solution but TMAO does not.[8,31] Note that the experimentally measured dipole moments of TMAO and TBA in apolar solutions are 5.04 Debye[53] and 1.76 Debye,[93] respectively, which are close to the calculated values. As discussed in ref. 5, the effective dipole moment of the hydrated TMAO–water complex is substantially higher (10.7 Debye).

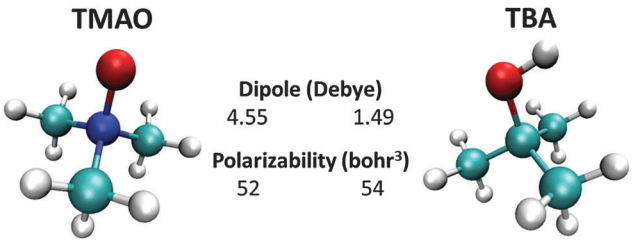

Fig. 1 Molecular structures of zwitterionic TMAO and neutral TBA, together with their gas-phase dipole moment and polarizability calculated at the M06/cc-PVTZ level of theory. Red, blue, sky blue, and white spheres denote the oxygen, nitrogen, carbon, and hydrogen atoms, respectively.

For TMAO, the dipole moment calculated from the electrostatic potential fitted charge[32] at the O_{TMAO} atom of $-0.629\ e$ and the N^+–O^- distance of 1.34 Å is 4.05 Debye, meaning that 90% of the dipole moment of TMAO is generated by the N^+–O^- part. Note that similar values have been reported in various studies.[33,34] This large dipole moment of the N^+–O^- part characterizes the hydrophilicity of the TMAO. In contrast, the molecular polarizabilities of TMAO and TBA are similar.

II-B. C–H stretching mode of the methyl group of TMAO

Understanding the vibrational nature of TMAO is essential to interpret the vibrational spectra and extract molecular level insight into the structure of TMAO from the vibrational data. In general, symmetric and anti-symmetric C–H stretching modes contribute to the optical spectra in the very narrow frequency range around 2900 cm^{-1}. In addition, the C–H stretching mode is often modulated by the overlap of the C–H stretching and the overtone of the H–C–H bending modes, which is called Fermi resonance.[35,36] The Fermi resonance peak often overlaps the peak of the anti-symmetric C–H stretching modes, which alters their peak intensities.[37] Vibrational mode assignments have been frequently made by performing *ab initio* harmonic calculations.[9] Since the anharmonic effect is not included in the harmonic calculation, the calculated frequencies are usually scaled to compensate the effects of anharmonicity of potential to the vibrational frequency.[38] In this scheme, we have used a common scaling factor for different vibrational modes.[39] Moreover, the harmonic calculations cannot address the contribution of the Fermi resonance, because they do not take into account any vibrational mode couplings. To address the anharmonic correction and the Fermi resonance, the vibrational Hamiltonian approach,[40,41] vibrational self-consistent field (VSCF) approach,[42–44] or perturbative approach[45] should be employed. The vibrational Hamiltonian approach is more computationally inexpensive, but it is more empirical than the VSCF-based approach.

We summarize the C–H stretching vibrational signature of TMAO calculated from the post-VSCF-based approach in Table 1. For a methyl group, three C–H stretching modes (symmetric, in-plane anti-symmetric, and out-of-plane anti-symmetric) contribute to the optical spectra at frequencies ranging from 2800 cm^{-1} to 3100 cm^{-1}. However, the frequencies of the C–H stretching modes vary substantially for each molecule; for methanol, the frequency difference between the symmetric mode and the in-plane anti-symmetric mode is $\sim$150 cm^{-1}, while it is $\sim$70 cm^{-1} for TMAO. The symmetric mode of methanol is 100 cm^{-1} lower than that of TMAO. Furthermore, the anti-symmetric in-plane mode can have a higher or lower frequency than the out-of-plane mode; for methanol, the in-plane mode provides a lower frequency than the out-of-plane mode, whereas it is reversed for TMAO. Table 1 also shows that the Fermi resonance frequency

Table 1 Vibrational frequencies in cm^{-1} of methanol, TBA, and TMAO calculated in this work at the level of second-order vibrational quasi-degenerate perturbation theory (VQDPT2)[46] using the SINDO program.[47] The harmonic, cubic, and quartic terms of semiquartic force fields were calculated at the B3LYP/6-311+G** level of theory. The experimentally reported gas phase frequencies[9,48,49] are given in parentheses

	Methanol	TBA	TMAO
Symmetric	2818 (2845)	2854–2922 (2880–2913)	2922–2928 (2952)
Fermi resonance	2919 (2925)	2930, 2945	2938
Out-of-plane anti-symmetric	2924 (2961)	2936–2955	3009–3015 (3036)
In-plane anti-symmetric	2972 (2980)	2940–2959	2989–2997 (3006–3018)

is very close to the out-of-plane antisymmetric mode frequency for methanol and TBA, while it is very close to the symmetric mode frequency for TMAO. As such, peak assignments of the C–H stretching mode are highly dependent on the molecules. Accurate quantum chemistry calculations beyond the harmonic calculations therefore seem to be necessary for correct peak assignment.

II-C. Modulation of the O–H stretching mode of water due to TMAO

The O–H stretching frequency of H_2O molecules (or O–D for D_2O molecules) is strongly dependent on the intermolecular interactions of water, in particular, hydrogen bond interactions; the strong hydrogen bond interaction lowers the O–H/O–D stretching frequency.[50] Through this sensitivity of the O–H/O–D stretching frequency to the molecular interactions, we can understand how the solute molecules affect the hydrogen bond structure of water.[50] As is displayed in Fig. 2(a), HOD dissolved in H_2O shows two bands in the 2100–2600 cm^{-1} range: a combination band at $\sim$2100 cm^{-1} and the O–D stretching mode at 2500 cm^{-1}. Addition of TMAO results in a strong increase of the absorption of the solutions at $\sim$2200–2400 cm^{-1},[5,51] indicative of red-shifted O–D oscillators. A similar red-shifted contribution to the O–H stretching band has been reported for a solution of TMAO in H_2O.[8] Thus, IR spectra indicate the presence of a strong hydrogen bond between TMAO and water. However, it is not clear how water molecules interact with TMAO and which interaction of water and TMAO gives rise to the low frequency O–H stretching band. High-level vibrational spectral simulations are clearly required to identify the molecular origin of the red-shift of the O–D stretching mode.[52]

Here, we identify which of the O–D groups that interact with TMAO cause the appearance of the band at $\sim$2200–2400 cm^{-1}. To do so, we categorized all the O–D groups of D_2O molecules in a simulation cell into the O–D groups near the hydrophilic O_{TMAO} atom (sub-ensemble G1), the O–D groups near the hydrophobic methyl group (G2), and the O–D groups that are away from TMAO (G3). These sub-ensembles are schematically depicted in Fig. 2(b).[19] By calculating the vibrational density of states for these sub-ensembles, we could assign the vibrational spectra to the specific ensemble. The simulated vibrational densities of states for the sub-ensembles G1 and G2 using AIMD trajectories are plotted in Fig. 2(c).[19] This indicates that the $\sim$200 cm^{-1} red-shifted band observed in IR spectra[5] arises from the strong hydrogen-bond of water's O–D group and the O_{TMAO} atom (sub-ensemble G1). On the other hand, the contribution of the O–D stretching chromophores near the hydrophobic group of TMAO almost completely overlaps with the bulk O–D stretching band (black line in Fig. 2(c)), making their contributions invisible in the O–D stretching vibrational spectra.

III. Hydration structure of and dynamics near TMAO

III-A. Time-resolved vibrational spectroscopy

Time-resolved pump–probe vibrational spectroscopy[52] has been used for understanding the hydration structure and dynamics near TMAO.[5,6,10,54–56] For example, by exciting and subsequently probing the vibrational modes with different light polarization combinations, one can monitor the rotational dynamics of molecules.[52] By applying this time-resolved vibrational approach to the O–D stretching mode of HDO in isotopically diluted aqueous TMAO solution, it was revealed that the rotational motions of the water molecules near TMAO are largely frozen.[5,6] Fig. 3 plots the

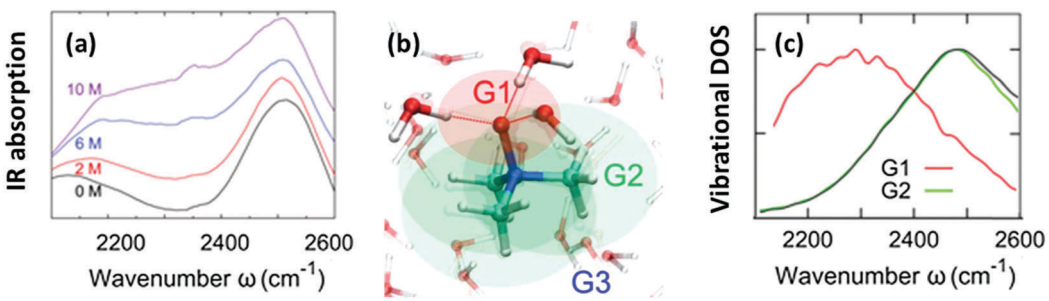

Fig. 2 (a) Vibrational IR spectra of the O–D stretching mode of isotopically diluted water (8% HDO in H_2O) at various concentrations of TMAO. Note that the small, narrow feature at 2350 cm^{-1} stems from the absorption of atmospheric CO_2. (b) Schematics of the categorization of water (G1, G2, and G3). (c) Simulated vibrational density of states for sub-ensembles G1 and G2 together with the vibrational density of states for pure D_2O (black line). Figures are adapted from ref. 5 and 19 with permission of the American Chemical Society.

decay of the orientation (anisotropy decay, defined later in eqn (1)) of the O–D group by pumping the low frequency side of the O–D stretching mode (left) and the high frequency side (right). These panels show very different anisotropy decays; for pumping at 2440 cm^{-1}, the anisotropy decay is very strongly slowed down with increasing TMAO concentration, while for pumping at 2560 cm^{-1}, the slowdown is less dramatic and changes more gradually. Since the low frequency O–D stretching mode originates from the O–D group hydrogen bonded to the O_{TMAO} atom as discussed in Section II, the frozen motion of water arises from the strong O–D$\cdots$$O_{TMAO}$ hydrogen bond. Further simulation evidence is given in the next subsection.

This dramatic slowing down of the water motion can be found not only for TMAO solution but also for tetramethylurea (TMU), proline, *N*-methylacetamide (NMA),[6] and TBA solutions.[54] This is evidenced not only by the anisotropy decay data but also from vibrational dynamics data obtained by two-dimensional IR (2DIR) spectroscopy. In 2DIR, the signals are plotted in contour maps by using two frequency axes – the excitation frequency (ω_1) and the probing frequency (ω_3).[29,50,52] In the two-dimensional contour map, the center line slope (CLS) of the diagonal peak is almost parallel to the diagonal line ($\omega_1 = \omega_3$) at $T = 0$ ps and becomes parallel to the ω_1 axis for long time T between excitation and probe pulses. By monitoring this CLS over time,[57] we can obtain information on the time-scale of the spectral diffusion, *i.e.* how fast the vibrational modes experience different frequencies. Fig. 4 shows the 2DIR spectra in the O–H stretch region for pure water, a TMAO solution, and a TBA solution for various waiting times T.[54] Clearly, the CLS of the diagonal peak changes rapidly for pure H_2O, while for the TMAO and TBA solutions, the CLS dynamics are slower. This again indicates that the vibrational dynamics of the O–H stretching mode slow down due to the presence of TMAO/TBA molecules, consistent with the conclusions from the anisotropy decay measurements.[6]

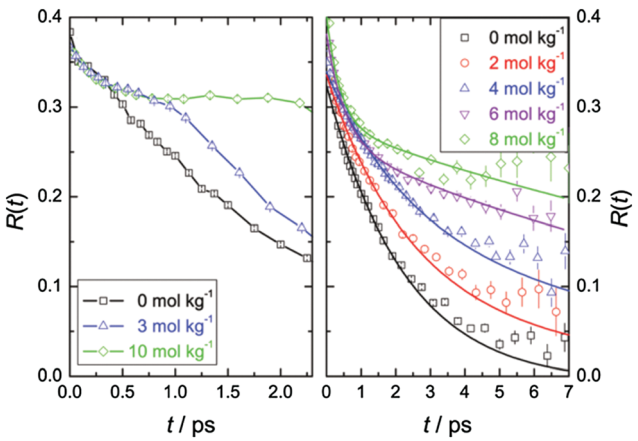

Fig. 3 (left) Anisotropy decay, $R(t)$, for the O–D vibration of HDO molecules in aqueous TMAO solutions with the pump pulse centered at around 2440 cm^{-1} for various TMAO concentrations. (right) $R(t)$ with the pump pulse centered at around 2560 cm^{-1}. Figures are adapted from ref. 5 with permission of the American Chemical Society.

III-B. Molecular dynamics simulations

The anisotropy decay can be computed from a MD simulation trajectory.[52] The anisotropy decay $R(t)$ of the O–D group of D_2O can be given by

$$R(t) = \frac{2}{5}\left\langle P_2\left(\frac{\mathbf{r}_{OD}(t)\cdot\mathbf{r}_{OD}(0)}{|\mathbf{r}_{OD}(t)||\mathbf{r}_{OD}(0)|}\right)\right\rangle \quad (1)$$

where $\mathbf{r}_{OD}(t)$ denotes the vector of the O–D group of the D_2O molecule at time t, and the second Legendre polynomial, $P_2(x) = \frac{1}{2}(3x^2 - 1)$. $R(t)$ calculated from the force field MD trajectories using the Kast model of TMAO[58] shows that the slowing down of the water orientation when TMAO is added to water is rather moderate.[16] This moderate slowing down can be attributed to the excluded volume effects of TMAO hydrophobic methyl groups which suppress the jump-like water reorientation.[59] However, this cannot account for the experimentally observed strong pump frequency dependence of the anisotropy decay of water.[5] Moreover, the MD simulations predicted that the addition of TMAO does not affect the IR spectra of the water O–H stretching mode,[17] which deviates strongly from the experimental data.[5] This questions the accuracy of the force field model of TMAO.[58] In fact, discrepancies between experimental data and simulated data with the Kast force field model[58] were reported and therefore many revised force field models of TMAO have been proposed.[60–63] In contrast to the force field MD, in AIMD simulations, the forces acting on the atoms are calculated based on electronic structure theory and therefore AIMD can be considered as a parameter-free technique. AIMD simulations would thus be a unique tool to re-examine the hydration structure and dynamics of TMAO.

To compare the anisotropy decay of the AIMD and force field MD, the left panel of Fig. 5 plots $R(t)$ calculated from the AIMD trajectories at the BLYP/TZV2P level of theory using the Grimme's D3 van der Waals correction[64] and the force field MD trajectories using the Kast force field model.[58] The anisotropy decay is decomposed to the O–D groups near the hydrophilic O_{TMAO} atom (sub-ensemble G1), the O–D groups near the hydrophobic methyl group (G2), and the O–D groups that are away from TMAO (G3), as discussed in Fig. 2(b). The simulated anisotropy data plotted in Fig. 5 show that the force field MD simulations predict a very quick decay for the G1 sub-ensemble, whereas the AIMD simulations predict a much slower G1 anisotropy decay. This indicates that the solvation dynamics in the AIMD simulations differ qualitatively from those in the force field MD simulations.[19] This difference in the force field MD and AIMD simulations arises from the sp^3 hybrid orbital of the O_{TMAO} atom; the hybrid orbital fixes the O–D$\cdots$$O_{TMAO}$ hydrogen bond direction, extending the hydrogen bond lifetime in the AIMD simulations, while this effect cannot be captured by the force field MD simulations.[19]

Subsequently, we turn our focus to the detailed dynamics of the G1 decay. The G1 decay may arise from the following two mechanisms: (i) the O–D groups are strongly hydrogen bonded to the O_{TMAO} atom and rotate together with the TMAO molecule (see (a) and (b) in the right panel of Fig. 5). The other scenario (ii) is that the O–D$\cdots$$O_{TMAO}$ hydrogen-bond is broken, and the

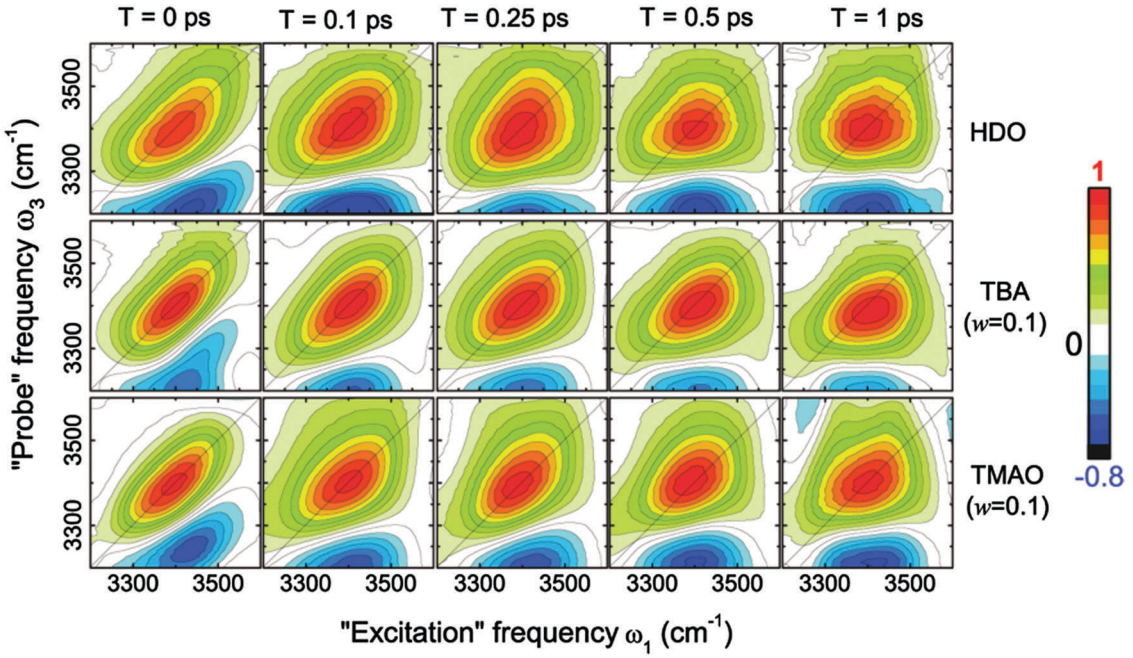

Fig. 4 Two-dimensional correlation spectra of pure HDO:D_2O and solutions of TBA and TMAO in HDO:D_2O at the concentration of 0.1 wt%, measured at different waiting times T. Figures are adapted from ref. 54 with permission of the American Chemical Society.

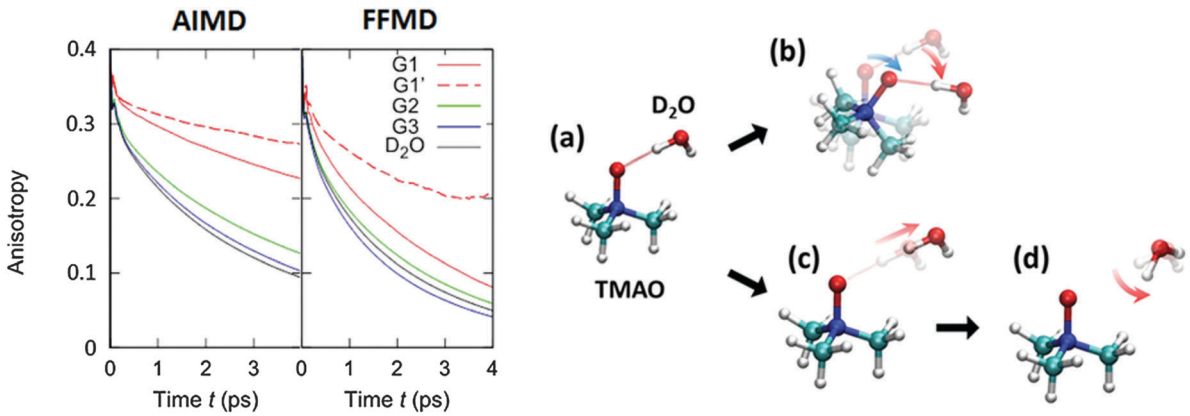

Fig. 5 (left) Simulated anisotropy decays of the G1, G2, and G3 O–D groups in aqueous TMAO solutions, obtained from AIMD and force field MD simulations. (right) Two mechanisms for the G1 O–D groups to lose their initial orientation. The upper route (a to b) shows the mechanism for the case that the O–D$\cdots$$O_{TMAO}$ hydrogen-bond remains intact, and reorientation occurs as the entire TMAO+D_2O complex rotates (denoted as sub-ensemble G1′), while the lower pathway (a, c, to d) shows the mechanism by which reorientation occurs by breaking of the hydrogen-bond and subsequent rotation of the O–D group. Figures are adapted from ref. 19 with permission of the American Chemical Society.

O–D group can subsequently rotate more freely in the bulk water (see pathways (a), (c) and (d) in the left panel of Fig. 5). To extract the effect of the mechanisms (i) on the rotational dynamics of G1 anisotropy decay, we simulated the anisotropy decay of those O–D groups within the G1 ensemble which keep the O–D$\cdots$$O_{TMAO}$ hydrogen-bond intact (sub-ensemble G1′); the difference in the G1 and G1′ anisotropy decay arises from mechanism (ii), while the G1′ decay arises solely from mechanism (i). The simulated G1′ anisotropy decay is represented by the broken red line in the right panel of Fig. 5. The G1′ decay is roughly half of the G1 decay, indicating that both the mechanisms (i) and (ii) ((a) to (b), and (a) to (c) and (d) in the left panel of Fig. 5) contribute to the anisotropy decay of water interacting with the O_{TMAO} atom.

Above, we show that AIMD simulations are very powerful to uniquely identify the structure and dynamics of water near the amphiphilic TMAO molecules. AIMD simulations have been applied not only for aqueous TMAO solutions but also for the aqueous solutions of other amphiphilic molecules.[65–68] In fact, the slowing down mechanism of water near the amphiphilic TMU molecule has been investigated, but the mechanism for TMU seems to differ from that of TMAO.[66] Ensing and co-workers found that the hydration dynamics near TMU are mainly attributed to the

water molecules located near the hydrophobic group.[66] As is commented in ref. 66, different hydration structures of TMAO and TMU may arise from the zwitterionic nature of TMAO and the polar nature of TMU. This requires further understanding of how hydrophilic the N–O group of TMAO and the C–O group of TMU are, and how hydrophobic the methyl groups of TMAO and TMU are.

IV. TMAO at the water–air interface: hydrophilicity *vs.* hydrophobicity

IV-A. C–H stretching SFG spectra

Above we discussed the water solvation dynamics near TMAO, when TMAO is fully solvated in the bulk. However, to examine the hydrophobicity/hydrophilicity of the specific part of TMAO, full solvation of TMAO is not ideal. Rather, placing TMAO at the interface consisting of hydrophobic/hydrophilic media and observing the orientation of TMAO with respect to the interface is very useful for examining the hydrophobicity/hydrophilicity of TMAO. The water–air interface is an ideal platform for this investigation. Here, to probe TMAO near the interface spectroscopically, we consider surface specific vibrational SFG spectroscopy[69,70] at the TMAO aqueous solution–air interface. The SFG signals are generated by overlapping an IR pulse and a visible pulse at the surface. Since the SFG optical process is a second-order nonlinear process, the signal from the centrosymmetric bulk vanishes, providing selectively the response from molecules located at the interfaces.[69,70] As such, we can selectively probe the molecular response near the interface.

To understand the orientation of TMAO at the water–air interface, we can probe either the C–H stretching mode or the N–O stretching mode with SFG. Interpreting the C–H stretching mode is more complicated, because of the energy splitting and Fermi resonance, as is discussed in Section II. Nevertheless, the C–H mode is frequently probed, as it is easily addressed with experiments. Here, we examine the orientation of the TMAO by focusing on the C–H stretching mode (Fig. 6).

The first attempt to identify the TMAO orientation at the water–air interface was conducted by Cremer and co-workers;[71] they performed the homodyne-detected SFG measurement for the aqueous TMAO solution–air interface and obtained the imaginary part of the second-order susceptibility ($\mathrm{Im}(\chi^{(2)}(\omega))$) from the SFG intensity data ($|\chi^{(2)}(\omega)|^2$)[71] using the maximum entropy method.[72,73] $\mathrm{Im}(\chi^{(2)}(\omega))$ provides the information on the absolute orientation (up-oriented toward air or down-oriented toward the bulk) with respect to the surface. Later, heterodyne detected SFG measurements have been conducted, which allow us to access $\mathrm{Im}(\chi^{(2)}(\omega))$ directly.[26,74] Furthermore, to remove the effects of the intra-/inter-molecular coupling of water on the SFG spectra, isotopically diluted water was used instead of neat water in the heterodyne-detected SFG measurement.[27]

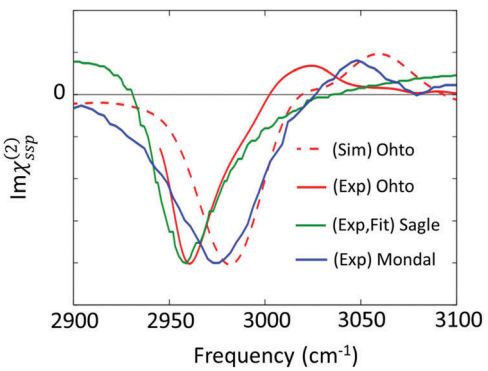

Fig. 6 Imaginary parts of SFG spectra for the C–H stretching mode at the aqueous TMAO solution–air interface reported in various papers (Ohto;[27] Sagle;[71] and Mondal[74]).

For the vibrational response of the methyl group of lipids and surfactants, the negative peak at the C–H symmetric stretching mode indicates that the C–H group points up to the air.[75] However, the vibrational mode assignment of TMAO is much more complicated, as is discussed in Section II and shown in Table 1; since the C–H symmetric stretching mode overlaps substantially with the C–H Fermi resonance, we have to be careful to conclude that the negative 2960–2980 cm^{-1} evidences that the methyl group points up to the air. In contrast to the complex interplay between the symmetric stretching mode and the Fermi resonance, the anti-symmetric mode is not affected by the Fermi resonance, meaning that this mode is suitable for determining the orientation of the methyl group of TMAO. The positive anti-symmetric in-plane mode manifests that the methyl group points up from the bulk water to the air.[27]

IV-B. O–H stretching SFG spectra

The effects of TMAO molecules on the O–H stretching mode of water in the SFG spectra have been interrogated through the comparison between the water–air interface and the aqueous TMAO solution–air interface.[26,27,71,74] Here, we overview the SFG signatures of the O–H stretching mode of water at the water–air interface in the presence of TMAO. The SFG spectra of water at the neat H_2O/air interface are displayed in Fig. 7(a) and (b), showing a 3400 cm^{-1} negative peak and the free O–H stretching peak at 3700 cm^{-1}. Note that after a long debate, the absence of the 3100 cm^{-1} positive SFG feature at the water–air interface has been agreed upon.[76,77]

We now turn our focus on the variation of the O–H stretching SFG spectra in the presence of the amine-*N*-oxide group. The SFG spectra of interfacial water in the presence of TMAO and dodecyl-dimethyl-amine-*N*-oxide surfactant (DDAO) molecules are shown in Fig. 7(a). For TMAO, the water response is indistinguishable from that of pure water; for DDAO, the SFG spectra in isotopically diluted water show a negative response very similar to that in pure water around 3400 cm^{-1}, and, in addition, an enhanced amplitude of the negative peak around 3500–3600 cm^{-1}. This distinct feature of the DDAO–surfactant case can be attributed to the absence of the free O–H positive peak, because the water–air interface is fully covered by the DDAO–surfactant, unlike the TMAO solution–air interface and the water–air interface. The similar 3200–3400 cm^{-1} SFG features of the TMAO solution and DDAO–surfactant–water interface indicate that the influence of the AO group on the water is independent of the length of the alkyl chains. This again manifests that the methyl

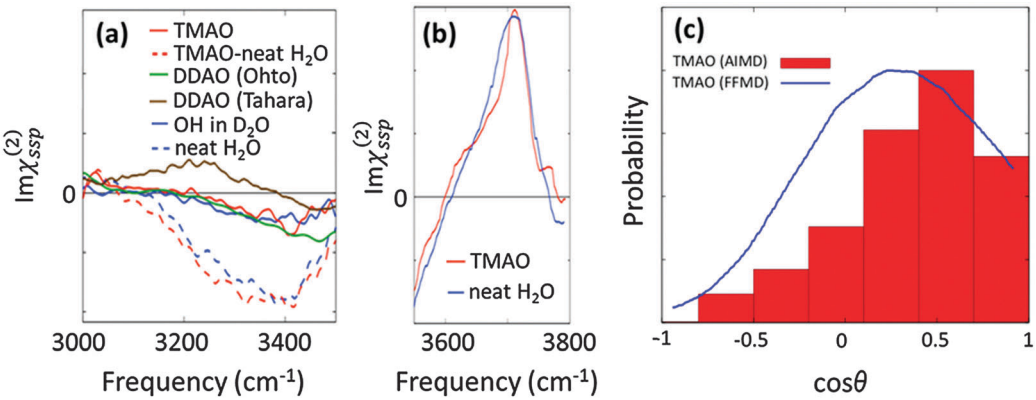

Fig. 7 (a) Experimental SFG spectra ($Im\chi^{(2)}_{ssp}(\omega)$) in the hydrogen bonded O–H stretching mode region. The TMAO solution–air interface for neat H_2O (red broken line) and isotopic diluted water (red solid line), the water/air interface for both pure water (blue broken line) and isotopic diluted water (blue solid line), and the DDAO/isotopic diluted water interface (green and line). The DDAO spectral amplitude was normalized to the same C–H negative amplitude as TMAO. Note that the frequency range covered in the experiment is given by the finite bandwidth of the IR pulse. The data are obtained from ref. 27, 74, 78, and 79. (b) Experimentally measured $Im\chi^{(2)}_{ssp}(\omega)$ for the free O–H stretching mode.[74] (c) Probability distribution of the angle formed by the N–O group of TMAO at the interface and the surface normal, which is denoted by red bars.[27] The angle distribution with the force field MD (3 M TMAO concentration) was taken from ref. 80 for comparison, and is shown as the blue line.

groups of TMAO are hydrophobic, like the alkyl chains of the AO–surfactant. Note that the SFG spectra at the DDAO–surfactant–water interface show a distinct feature between ref. 27 and 78; ref. 78 reports the presence of a $\sim$3200 cm^{-1} positive peak which is missing in ref. 27. This should be addressed in future work.

Above, we have learned that TMAO is present near the interface and therefore the SFG signal of TMAO is non-zero. The remaining question is whether TMAO is excluded from the topmost water layer at the water–air interface and located in the near bulk region or really in the outermost surface region. In both AIMD and force field MD simulations, TMAO molecules can be found in the topmost layer of the water interface. This, however, contradicts the conclusion drawn from SFG spectra showing that the free O–H stretching SFG band of water is insensitive to the presence/absence of TMAO (see Fig. 7(b)). Mondal and co-workers attributed this insensitivity to an equal number of free O–H stretching chromophores present at the TMAO–solution/air and water/air interfaces,[74] and concluded that TMAO is therefore not present at the topmost water layer.

However, the SFG signal is proportional to both the number of vibrational chromophores in the laser spot and the orientation of the transition dipole moment. Thus, for attributing an invariance of O–H stretching SFG signal to an equal number of O–H stretching chromophores at the topmost water layer, one needs to assume that the orientation of the transition dipole moment is unchanged upon adding TMAO. With experimental tools, it is quite difficult to disentangle the variation of the number of chromophores and the variation of the molecular orientation as a result of the possible presence of TMAO. Therefore, again, a combination of SFG and MD simulations would be very powerful to uniquely address the molecular conformation near the interfaces. Such a combined experimental and simulation study indeed reveals that, despite the free O–H signal not changing upon addition of TMAO, TMAO is present in the outermost surface region, and, for the SFG response, the reduction in the number of free O–H groups is compensated by their increased orientation.

This conclusion was drawn from calculating the axial profiles of the average angle formed by the free O–H group and the surface normal for the water–air interface and the TMAO–solution–air interface. These are plotted in Fig. 7(c). Here, we define the free O–H group whose hydrogen atom cannot find any intermolecular oxygen atom within a 3.3 Å cutoff sphere. The data indicate that the angular distribution of the free O–H groups is indeed affected by the presence of TMAO; due to TMAO, the O–H groups point more up to the air. As such, although some free O–H groups are displaced by TMAO, and the number of free O–H groups is accordingly reduced, the free O–H stretching SFG signal seems invariant, due to the enhanced up-orientation of the remaining free O–H groups. This clearly demonstrates that the TMAO methyl groups are hydrophobic and are present near the hydrophobic surface, despite the free O–H signal remaining constant.

V. Outlook of TMAO research

V-A. TMAO–urea interaction in an aqueous environment

TMAO or other amine-oxides are found to counter the osmotic stress due to urea.[81–83] Intriguingly, in many marine environments both osmolytes are found in a rather well-defined stoichiometric ratio of 1 : 2 (TMAO : urea).[83] Indeed, the activity of many enzymes seems to be unaffected when TMAO and urea are present at a 1 : 2 ratio,[83] while for some biomolecules higher amounts of TMAO are required to compensate the osmotic stress of urea.[84–86] It is well established that urea is an efficient protein denaturant and that TMAO can efficiently stabilize proteins. Nevertheless, the observed compensation of both effects at this 1 : 2 ratio has stimulated many studies aiming

at exploring the underlying molecular-level interactions, which balance the physiological effects of both osmolytes at this stoichiometry.

While some evidence exists for direct complexation between TMAO and urea in bulk solution,[18,87] other studies[82,85,88] indicate that TMAO–urea contacts in solution are not more frequent than what would be expected based on random collisions. In line with this notion, experimental and theoretical studies arrived at the conclusion that TMAO and urea can be considered independent of each other in bulk and that there is no evidence for specific interactions between those two molecules being the origin of the counteraction.[13,89–92] Although there seems to be no specific direct interaction between TMAO and urea in bulk, indirect effects mediated *via* water have been reported.[55,82] In this context a detailed study of the behavior of mixed TMAO:urea solutions at interfaces is of particular interest, as the water hydrogen-bonded network, which mediates such indirect effects in bulk, is very different at interfaces. Indeed, classical MD simulations suggest that the situation of TMAO and urea may be drastically different if an interface is present,[94,95] while it needs to be stressed that for such studies the choice of the force-field models is extremely critical.[94,96] Therefore, only advances in both experimental methods and computational studies will be able to shed light on the underlying mechanisms for such complex multi-component systems.

V-B. Role of TMAO at water–protein interfaces

The variation of the biological function due to the presence of TMAO is directly linked with the molecular interaction of TMAO with proteins. The stabilization mechanism of protein structures has been intensively discussed with MD simulation techniques.[80,97–100] Using the Kast force field model,[58] Thirumalai and co-workers have demonstrated that TMAO limits the degrees of freedom for the unfolded conformation of proteins, making the folded state more preferable.[98] However, as is discussed in Section III-B, the Kast model has serious drawbacks for describing the hydrogen-bonding dynamics and hydration structure. These may affect the stabilization mechanism of protein folding. In fact, Garcia and co-workers have shown that the Kast model of TMAO does not show preferable exclusion from the protein surface.[62] For the careful assessment of the TMAO–urea and TMAO–protein interactions, the development of an accurate force field model is crucial.[60–63] The AIMD data discussed above can offer a unique check for the developed force field model of TMAO.

Experimentally, the protein folding/unfolding dynamics have been investigated by time-resolved vibrational spectroscopy including 2DIR spectroscopy. Gai and co-workers conducted 2DIR measurement for the TMAO–protein system by probing the C–N stretch mode of an unnatural amino acid.[101,102] The results indicate two possible mechanisms: TMAO decreases the hydrogen bonding ability of water, stabilizing the unfolded state or TMAO acts as a molecular crowder, increasing the stability of the folded state *via* the excluded volume effect.[98,101] Such a solvent-excluded volume effect in the stabilizing action of TMAO has also been revealed *via* an approach based on classical scaled particle modelling.[103,104] MD simulations investigating these possible mechanisms would be again critically dependent on the accuracy of the force field model of TMAO and the interactions between TMAO and proteins in the force field MD simulations. Therefore, we need to combine spectroscopy with simulations to gain accurate molecular level insight into the TMAO–protein interactions. Typical questions concerning the effect of TMAO on proteins include: how does TMAO stabilize the protein structure? Does TMAO affect the hydrogen bond network around proteins, *e.g. via* binding of available water molecules? Does the roughness of the protein surface enhance or suppress the activity of TMAO with regard to protein (de-)stabilization?

To answer the question of how TMAO affects proteins, we need to understand the orientation of TMAO with respect to the protein–water interface. To do so, the SFG technique would be again useful; when TMAO can interact with a specific site of a protein, TMAO can have a specific orientation resulting in a non-zero SFG signal. As such, we will be able to probe the TMAO near the protein surface selectively by SFG spectroscopy and be able to learn the orientation of TMAO.

For monitoring the association dynamics of TMAO, the chemical exchange type of two-dimensional SFG (2DSFG) would be useful. In fact, this chemical exchange 2DIR technique has been used for over 10 years,[105,106] though it has not been applied for 2DSFG. In the chemical exchange 2DIR technique, different vibrational frequencies for associated and dissociated conformations of the TMAO–protein system generate an off-diagonal peak in the two-dimensional spectra. Monitoring the creation and annihilation of this off-diagonal peak provides information on the speed of the chemical exchanges. Chemical exchange 2DSFG would be not only powerful to address the TMAO–protein association dynamics but also to monitor the association–dissociation liquid dynamics at the interfaces.

Finally, we comment on the previous combined studies of MD simulations and SFG spectroscopy at the water–protein interfaces. Since both SFG and MD can address the bond orientations and conformation of the protein, these techniques have been successfully combined.[107–111] Moreover, the recent advances in MD simulations allow us to calculate the SFG spectra and compare the simulated SFG spectra with the experimentally measured spectra.[112,113] Information on the orientational motion obtained from time-resolved data is also compared with the simulation data.[114] These would be powerful tools to achieve a tight collaboration between MD simulation and SFG spectroscopy, contributing to the sophistication of the force field models and an accurate description of the protein–TMAO interactions.

VI. Concluding remarks

We have provided an overview of recent progress on the solvation structure and dynamics of water near TMAO and other amphiphilic molecules. In particular, we focus on vibrational spectroscopy and simulation studies. Several mysteries have been unveiled by combining MD simulations with vibrational spectroscopy. The hydrophilic part of TMAO forms exceptionally strong hydrogen-bonds with water, which results in a strongly red-shifted

contribution to the O–H stretching band in the vibrational spectrum. These strong hydrogen bonds are important to understand TMAO's function as a molecular crowder as the strong interaction can reduce the number of water molecules that are available to hydrate a biomolecule. These strong hydrogen-bonds are also at the heart of the slowing down of the water molecules' motion near TMAO. The vibrational/computational (mainly AIMD simulation) study unambiguously revealed that the slowing down of the rotation of the O–H groups arises from the O–H group interacting with the O_{TMAO} atom rather than from hydrophobic hydration of methyl groups of TMAO nor from the excluded volume effects due to the hydrophobic methyl group.

The other highlight is uncovering the nature of the methyl group of TMAO. This can be characterized by placing TMAO at the water–air interface; the orientation and location of TMAO can be linked to the hydrophobicity/hydrophilicity of TMAO. The orientation of TMAO can be determined from the sign of the imaginary part of the SFG spectra. The combined SFG measurement and AIMD simulations revealed that the N–O_{TMAO} group of TMAO points down to the water phase. Moreover, TMAO can be found at the water–air interface, manifesting that the methyl group of TMAO is hydrophobic rather than hydrophilic. Finally, we believe that the combination of vibrational spectroscopy and simulation techniques can play an important role in unveiling molecular insights into TMAO–protein and TMAO–urea interactions.

Competing financial interest

The authors declare no competing financial interest.

Acknowledgements

We are grateful to Helmut Lutz and Wenjun Xie for fruitful discussion. Open Access funding provided by the Max Planck Society.

References

1 P. H. Yancey, *J. Exp. Biol.*, 2005, **208**, 2819–2830.
2 A. D. M. Dove, J. Leisen, M. Zhou, J. J. Byrne, K. Lim-hing, H. D. Webb, L. Gelbaum, M. R. Viant, J. Kubanek and F. M. Ferna, *PLoS One*, 2012, **7**, e49379.
3 C. Krywka, C. Sternemann, M. Paulus, M. Tolan, C. Royer and R. Winter, *ChemPhysChem*, 2008, **9**, 2809–2815.
4 J. L. Silva, A. C. Oliveira, T. C. Vieira, G. A. de Oliveira, M. C. Suarez and D. Foguel, *Chem. Rev.*, 2014, **114**, 7239–7267.
5 J. Hunger, K. J. Tielrooij, R. Buchner, M. Bonn and H. J. Bakker, *J. Phys. Chem. B*, 2012, **116**, 4783–4795.
6 Y. L. A. Rezus and H. J. Bakker, *Phys. Rev. Lett.*, 2007, **99**, 148301.
7 K. A. Sharp, B. Madan, E. Manas and J. M. Vanderkooi, *J. Chem. Phys.*, 2001, **114**, 1791–1796.
8 M. Freda, G. Onori and A. Santucci, *J. Phys. Chem. B*, 2001, **105**, 12714–12718.
9 K. L. Munroe, D. H. Magers and N. I. Hammer, *J. Phys. Chem. B*, 2011, **115**, 7699–7707.
10 K. Mazur, I. a. Heisler and S. R. Meech, *Phys. Chem. Chem. Phys.*, 2012, **14**, 6343–6351.
11 R. Sinibaldi, C. Casieri, S. Melchionna, G. Onori, A. L. Segre, S. Viel, L. Mannina and F. De Luca, *J. Phys. Chem. B*, 2006, **110**, 8885–8892.
12 J. Qvist and B. Halle, *J. Am. Chem. Soc.*, 2008, **130**, 10345–10353.
13 C. J. Sahle, M. A. Schroer, I. Juurinen and J. Niskanen, *Phys. Chem. Chem. Phys.*, 2016, **18**, 16518–16526.
14 Y. Sasaki, Y. Horikawa, T. Tokushima, K. Okada, M. Ourab and M. Aida, *Phys. Chem. Chem. Phys.*, 2016, **18**, 27648–27653.
15 T. Shikata and S. Itatani, *J. Solution Chem.*, 2002, **31**, 823–844.
16 D. Laage, G. Stirnemann and J. T. Hynes, *J. Phys. Chem. B*, 2009, **113**, 2428–2435.
17 G. Stirnemann, J. T. Hynes and D. Laage, *J. Phys. Chem. B*, 2010, **114**, 3052–3059.
18 S. Paul and G. N. Patey, *J. Am. Chem. Soc.*, 2007, **129**, 4476–4482.
19 K. Usui, J. Hunger, M. Sulpizi, T. Ohto, M. Bonn and Y. Nagata, *J. Phys. Chem. B*, 2015, **119**, 10597–10606.
20 J. L. Finney, D. T. Bowron, R. M. Daniel, P. A. Timmins and M. A. Roberts, *Biophys. Chem.*, 2003, **105**, 391–409.
21 P. Buchanan, N. Aldiwan, A. K. Soper, J. L. Creek and C. A. Koh, *Chem. Phys. Lett.*, 2005, **415**, 89–93.
22 N. Galamba, *J. Phys. Chem. B*, 2014, **117**, 2153–2159.
23 G. Graziano, *J. Phys. Chem. B*, 2014, **118**, 2598–2599.
24 N. Galamba, *J. Phys. Chem. B*, 2014, **118**, 2600–2603.
25 Y. Koga, P. Westh, K. Nishikawa and S. Subramanian, *J. Phys. Chem. B*, 2011, **115**, 2995–3002.
26 J. A. Mondal, *J. Phys. Chem. Lett.*, 2016, **7**, 1704–1708.
27 T. Ohto, E. H. G. Backus, W. Mizukami, J. Hunger, M. Bonn and Y. Nagata, *J. Phys. Chem. C*, 2016, **120**, 17435–17443.
28 D. Marx and J. Hutter, *Ab initio molecular dynamics: basic theory and advanced methods*, Cambridge University Press, 2009.
29 S. Mukamel, *Annu. Rev. Phys. Chem.*, 2000, **51**, 691–729.
30 M. W. Schmidt, K. K. Baldridge, J. A. Boatz, S. T. Elbert, M. S. Gordon, J. H. Jensen, S. Koseki, N. Matsunaga, K. A. Nguyen, S. Su, T. L. Windus, M. Dupuis and J. A. Montgomery, *J. Comput. Chem.*, 1993, **14**, 1347–1363.
31 S. Paul and G. N. Patey, *J. Phys. Chem. B*, 2006, **110**, 10514–10518.
32 S. R. Cox and D. E. Williams, *J. Comput. Chem.*, 1981, **2**, 304–323.
33 V. Kocherbitov, V. Veryazov and O. Söderman, *J. Mol. Struct. THEOCHEM*, 2007, **808**, 111–118.
34 I. M. Pazos and F. Gai, *J. Phys. Chem. B*, 2012, **116**, 12473–12478.
35 R. G. Snyder, H. L. Strauss and C. A. Elliger, *J. Phys. Chem.*, 1982, **86**, 5145–5150.
36 S. Abbate, S. L. Wunder and G. Zerbi, *J. Phys. Chem.*, 1984, **88**, 593–600.
37 S. Abbate, G. Zerbi and S. L. Wunder, *J. Phys. Chem.*, 1982, **86**, 3140–3149.

38 A. P. Scott and L. Radom, *J. Phys. Chem.*, 1996, **100**, 16502–16513.
39 I. M. Alecu, J. Zheng, Y. Zhao and D. G. Truhlar, *J. Chem. Theory Comput.*, 2010, **6**, 2872–2887.
40 H. M. Chase, B. Rudshteyn, B. T. Psciuk, M. A. Upshur, B. F. Strick, R. J. Thomson, V. S. Batista and F. M. Geiger, *J. Phys. Chem. B*, 2016, **120**, 1919–1927.
41 J. Ho, B. T. Psciuk, H. M. Chase, B. Rudshteyn, M. A. Upshur, L. Fu, R. J. Thomson, H. Wang, F. M. Geiger and V. S. Batista, *J. Phys. Chem. C*, 2016, **120**, 12578–12589.
42 T. K. Roy and R. B. Gerber, *Phys. Chem. Chem. Phys.*, 2013, **15**, 9468–9492.
43 J. M. Bowman, *Acc. Chem. Res.*, 1986, **19**, 202–208.
44 O. Christiansen, *Phys. Chem. Chem. Phys.*, 2012, **14**, 6672–6687.
45 J. Bloino and V. Barone, *J. Chem. Phys.*, 2012, **136**, 124108.
46 K. Yagi, S. Hirata and K. Hirao, *Phys. Chem. Chem. Phys.*, 2008, **10**, 1781–1788.
47 K. Yagi and H. Otaki, *SINDO 3.6*, RIKEN, 2014.
48 Y. Yu, Y. Wang, K. Lin, N. Hu, X. Zhou and S. Liu, *J. Phys. Chem. A*, 2013, **117**, 4377–4384.
49 J. Korppi-tommola, *Spectrochim. Acta*, 1978, **34**, 1077–1085.
50 F. Perakis, L. De Marco, A. Shalit, F. Tang, Z. R. Kann, T. D. Ku, R. Torre, M. Bonn and Y. Nagata, *Chem. Rev.*, 2016, **116**, 7590–7607.
51 A. Panuszko, P. Bruździak, J. Zielkiewicz, D. Wyrzykowski and J. Stangret, *J. Phys. Chem. B*, 2009, **113**, 14797–14809.
52 H. J. Bakker and J. L. Skinner, *Chem. Rev.*, 2010, **110**, 1498–1517.
53 E. P. Linton, *J. Am. Chem. Soc.*, 1940, **62**, 1945–1948.
54 A. A. Bakulin, M. S. Pshenichnikov, H. J. Bakker and C. Petersen, *J. Phys. Chem. A*, 2011, **115**, 1821–1829.
55 Y. L. A. Rezus and H. J. Bakker, *J. Phys. Chem. B*, 2009, **113**, 4038–4044.
56 K. Mazur, I. A. Heisler and S. R. Meech, *J. Phys. Chem. B*, 2011, **115**, 2563–2573.
57 K. Kwak, S. Park, I. J. Finkelstein and M. D. Fayer, *J. Chem. Phys.*, 2007, **127**, 124503.
58 K. M. Kast, J. Brickmann, S. M. Kast and R. S. Berry, *J. Phys. Chem. A*, 2003, **107**, 5342–5351.
59 D. Laage and J. T. Hynes, *Science*, 2006, **311**, 832–835.
60 E. Schneck, D. Horinek and R. R. Netz, *J. Phys. Chem. B*, 2013, **117**, 8310–8321.
61 L. Larini and J.-E. Shea, *J. Phys. Chem. B*, 2013, **117**, 13268–13277.
62 D. R. Canchi, P. Jayasimha, D. C. Rau, G. I. Makhatadze and A. E. Garcia, *J. Phys. Chem. B*, 2012, **116**, 12095–12104.
63 C. Hölzl, P. Kibies, S. Imoto, R. Frach, S. Suladze, R. Winter, D. Marx, D. Horinek and S. M. Kast, *J. Chem. Phys.*, 2016, **144**, 144104.
64 S. Grimme, J. Antony, S. Ehrlich and H. Krieg, *J. Chem. Phys.*, 2010, **132**, 154104.
65 J. T. Titantah and M. Karttunen, *J. Am. Chem. Soc.*, 2012, **134**, 9362–9368.
66 W. H. Brandeburgo, S. T. van der Post, E. J. Meijer and B. Ensing, *Phys. Chem. Chem. Phys.*, 2015, **17**, 24968–24977.
67 S. Imoto, H. Forbert and D. Marx, *Phys. Chem. Chem. Phys.*, 2015, **17**, 24224–24237.
68 J. T. Titantah and M. Karttunen, *Sci. Rep.*, 2013, **3**, 2991.
69 Y. R. Shen, *Nature*, 1989, **337**, 519–525.
70 M. Bonn, Y. Nagata and E. H. G. Backus, *Angew. Chemie Int. Ed.*, 2015, **54**, 5560–5576.
71 L. B. Sagle, K. Cimatu, V. a. Litosh, Y. Liu, S. C. Flores, X. Chen, B. Yu and P. S. Cremer, *J. Am. Chem. Soc.*, 2011, **133**, 18707–18712.
72 M. Sovago, E. Vartiainen and M. Bonn, *J. Phys. Chem. C*, 2009, **113**, 6100–6106.
73 A. G. F. de Beer, J.-S. Samson, W. Hua, Z. Huang, X. Chen, H. C. Allen and S. Roke, *J. Chem. Phys.*, 2011, **135**, 224701.
74 M. Ahmed, V. Namboodiri, P. Mathi, A. K. Singh and J. A. Mondal, *J. Phys. Chem. C*, 2016, 10252–10260.
75 S. Nihonyanagi, S. Yamaguchi and T. Tahara, *J. Chem. Phys.*, 2009, **130**, 204704.
76 T. Ohto, K. Usui, T. Hasegawa, M. Bonn and Y. Nagata, *J. Chem. Phys.*, 2015, **143**, 124702.
77 S. Yamaguchi, *J. Chem. Phys.*, 2015, **143**, 34202.
78 J. A. Mondal, S. Nihonyanagi, S. Yamaguchi and T. Tahara, *J. Am. Chem. Soc.*, 2012, **134**, 7842–7850.
79 T. Ohto, E. H. G. Backus, C.-S. Hsieh, M. Sulpizi, M. Bonn and Y. Nagata, *J. Phys. Chem. Lett.*, 2015, **6**, 4499–4503.
80 A. Fiore, V. Venkateshwaran and S. Garde, *Langmuir*, 2013, **29**, 8017–8024.
81 B. J. Bennion and V. Daggett, *Proc. Natl. Acad. Sci. U. S. A.*, 2004, **101**, 6433–6438.
82 J. Hunger, N. Ottosson, K. Mazur, M. Bonn and H. J. Bakker, *Phys. Chem. Chem. Phys.*, 2015, **17**, 298–306.
83 P. H. Yancey and G. N. Somero, *J. Exp. Zool.*, 1980, **212**, 205–213.
84 H. R. Palmer, J. J. Bedford, J. P. Leader and R. A. Smith, *J. Biol. Chem.*, 2000, **275**, 27708–27711.
85 L. M. Samuelsson, J. J. Bedford, R. A. J. Smith and J. P. Leader, *Comp. Biochem. Physiol. A. Mol. Integr. Physiol.*, 2005, **141**, 22–28.
86 T. C. Gluick and S. Yadav, *J. Am. Chem. Soc.*, 2003, **125**, 4418–4419.
87 F. Meersman, D. Bowron, A. K. Soper and M. H. J. Koch, *Biophys. J.*, 2009, **97**, 2559–2566.
88 F. Meersman, D. Bowron, A. K. Soper and M. H. J. Koch, *Phys. Chem. Chem. Phys.*, 2011, **13**, 13765.
89 H. Kokubo, C. Y. Hu and B. M. Pettitt, *J. Am. Chem. Soc.*, 2011, **133**, 1849–1858.
90 J. Mondal, D. Halverson, I. T. S. Li, G. Stirnemann, G. C. Walker and B. J. Berne, *Proc. Natl. Acad. Sci. U. S. A.*, 2015, **112**, 9270–9275.
91 J. Rösgen and R. Jackson-Atogi, *J. Am. Chem. Soc.*, 2012, **134**, 3590–3597.
92 M. Lever, K. Randall and E. A. Galinski, *Biochim. Biophys. Acta*, 2001, **1528**, 135.
93 U. S. Mohapatra, G. S. Roy and S. K. Dash, *Phys. Chem. Liquids*, 2001, **39**, 443–451.
94 P. Ganguly, N. F. A. van der Vegt and J.-E. Shea, *J. Phys. Chem. Lett.*, 2016, **7**, 3052–3059.

95 P. Ganguly, T. Hajari, J.-E. Shea and N. F. A. van der Vegt, *J. Phys. Chem. Lett.*, 2015, **6**, 581–585.
96 G. Borgohain and S. Paul, *J. Phys. Chem. B*, 2016, **120**, 2352–2361.
97 Q. Zou, B. J. Bennion, V. Daggett and K. P. Murphy, *J. Am. Chem. Soc.*, 2002, **124**, 1192–1202.
98 S. S. Cho, G. Reddy, J. E. Straub and D. Thirumalai, *J. Phys. Chem. B*, 2011, **115**, 13401–13407.
99 Z. A. Levine, L. Larini, N. E. LaPointe, S. C. Feinstein and J.-E. Shea, *Proc. Natl. Acad. Sci. U. S. A.*, 2015, **112**, 2758–2763.
100 Y. Yang, Y. Mu and W. Li, *Phys. Chem. Chem. Phys.*, 2016, **18**, 22081–22088.
101 J. Ma, I. M. Pazos and F. Gai, *Proc. Natl. Acad. Sci. U. S. A.*, 2014, **111**, 8476–8481.
102 B. Ding, M. R. Hilaire and F. Gai, *J. Phys. Chem. B*, 2016, **120**, 5103–5113.
103 G. Graziano, *Phys. Chem. Chem. Phys.*, 2011, **13**, 17689–17695.
104 G. Graziano, *Phys. Chem. Chem. Phys.*, 2012, **14**, 13088.
105 Y. S. Kim and R. M. Hochstrasser, *Proc. Natl. Acad. Sci. U. S. A.*, 2005, **102**, 11185–11190.
106 J. Zheng, K. Kwak, J. B. Asbury, C. Xin and M. D. Fayer, *Science*, 2005, **305**, 61–66.
107 D. Schach, C. Globisch, S. J. Roeters, S. Woutersen, A. Fuchs, C. K. Weiss, E. H. G. Backus, K. Landfester, M. Bonn, C. Peter and T. Weidner, *J. Chem. Phys.*, 2014, **141**, 22D517.
108 A. P. Boughton, I. Andricioaei and Z. Chen, *Langmuir*, 2010, **26**, 16031–16036.
109 A. P. Boughton, K. Nguyen, I. Andricioaei and Z. Chen, *Langmuir*, 2011, **27**, 14343.
110 H. Lutz, V. Jaeger, R. Berger, M. Bonn, J. Pfaendtner and T. Weidner, *Adv. Mater. Interfaces*, 2015, **2**, 1500282.
111 B. Ding, A. Panahi, J. J. Ho, J. E. Laaser, C. L. Brooks, M. T. Zanni and Z. Chen, *J. Am. Chem. Soc.*, 2015, **137**, 10190–10198.
112 J. K. Carr, L. Wang, S. Roy and J. L. Skinner, *J. Phys. Chem. B*, 2014, **119**, 8969–8983.
113 R. Pandey, K. Usui, R. A. Livingstone, S. A. Fischer, J. Pfaendtner, E. H. G. Backus, Y. Nagata, J. Fröhlich-nowoisky, L. Schmüser, S. Mauri, J. F. Scheel, D. A. Knopf, U. Pöschl, M. Bonn and T. Weidner, *Sci. Adv.*, 2016, **2**, e1501630.
114 M. A. Donovan, Y. Y. Yimer, J. Pfaendtner, E. H. G. Backus, M. Bonn and T. Weidner, *J. Am. Chem. Soc.*, 2016, **138**, 5226–5229.